Modelling segregation of bidisperse granular mixtures varying simultaneously in size and density for free surface flows

Yifei Duan, Paul B. Umbanhowar, Julio M. Ottino, Richard M. Lueptow†

Supplementary Material

1. DEM contact model

A linear spring-dashpot interaction model is used to calculate inter-particle collisional forces at the point of contact (Cundall & Strack 1979). For a pair of colliding spheres (indicated by subscripts j, k) the normal contact force is

$$\boldsymbol{F}_{jk}^n = [k_n\epsilon - 2\gamma_n m_{eff}(\boldsymbol{V}_{jk}\cdot\hat{\boldsymbol{r}}_{jk})]\hat{\boldsymbol{r}}_{jk}, \tag{1.1}$$

where $\hat{\boldsymbol{r}}_{jk}$ is the normal unit vector, $m_{eff} = m_k m_l/(m_k+m_l)$ is the effective mass, and ϵ and $\boldsymbol{V}_{jk}$ are the overlap and relative velocity between the two spheres, respectively. The normal stiffness

$$k_n = [(\pi/t_c)^2 + \gamma_n^2]m_{eff} \tag{1.2}$$

and damping

$$\gamma_n = -\ln(e)/t_c \tag{1.3}$$

are determined from the restitution coefficient e and binary collision time t_c. The tangential force is specified by a linear spring model with Coulomb friction (Shäfer *et al.* 1996)

$$\boldsymbol{F}_{jk}^t = -\min(|k_s\beta|, |\mu\boldsymbol{F}_{jk}^n|)\mathrm{sgn}(\beta)\hat{\boldsymbol{s}}. \tag{1.4}$$

Here $\hat{\boldsymbol{s}}$ is the unit vector in the tangential direction. The tangential stiffness is $k_s = \frac{2}{7}k_n$, and the tangential displacement magnitude is

$$\beta(t) = \int_{t_s}^{t} V_{jk}^s dt, \tag{1.5}$$

where t_s is the initial contact time and V_{jk}^s is the relative tangential velocity. The numerical implementation of equation (1.5) is provided elsewhere (Weinhart *et al.* 2020).

2. Collisional diffusion

The time evolution of the mean-squared displacement in the normal direction, MSD_z, for particles at approximately the same streamwise position ($x/L = 0.5$) but different depths ($z/\delta = -0.1$, -0.3, -0.5, -0.7, -0.9) is plotted in figure 2.1(a). As expected, the mean-squared displacement increases with time interval Δt at all five positions, and decreases with increasing depth at all times. The best fit line for each data set has a slope greater than 1 at smaller time intervals but a slope of 1 at larger time intervals,

† Email address for correspondence: r-lueptow@northwestern.edu

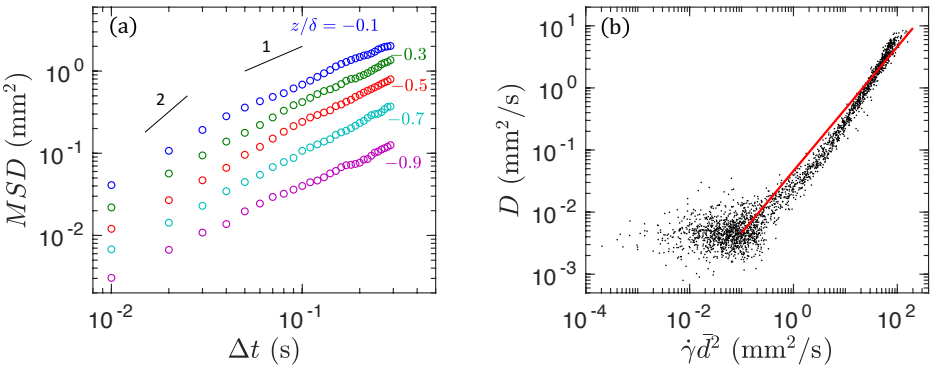

FIGURE 2.1. (a) MSD vs. Δt at different depths at $x/L = 0.5$. (b) D vs. $\dot{\gamma}\bar{d}^2$ [see equation (2.8)]. Line represents the best fit $0.046\dot{\gamma}\bar{d}^2$ for $\dot{\gamma}\bar{d}^2 > 0.1$. Only data for $x/L > 0.1$ and $z/\delta > -3$ are plotted. $R_d = 2$, $R_\rho = 4$, and $\hat{c}_l = 0.5$.

indicating that particle motion is diffusive for large Δt and super-diffusive (approaching ballistic) for small Δt as expected.

The diffusion coefficient of the mixture, D, is estimated as one-half of the slope of the best fit line to MSD_z versus Δt in the range 0.05 s to 0.3 s. In addition, D is plotted as a function of $\dot{\gamma}\bar{d}^2$ in figure 2.1(b). The approximately linear dependence of D on $\dot{\gamma}\bar{d}^2$ in the dense rapid flow regime ($\dot{\gamma}\bar{d}^2 > 0.1$) and the slope of the fitting line are consistent with previous studies (Fan *et al.* 2015). Deviation of the data points from the fitting line for $\dot{\gamma}\bar{d}^2 > 0.1$ could be a result of varying total solid volume fraction (ϕ_{total}) across the flowing layer, as previous studies of uniform shear flows show that the diffusion coefficient varies with ϕ_{total} in addition to $\dot{\gamma}\bar{d}^2$ (Cai *et al.* 2019).

3. Segregation model coefficients

As described with respect to figure 9 of the paper, it is difficult to collapse the data for the model coefficients A_l and B_l using a principled approach. Nevertheless, it is possible to devise empirical expressions for these coefficients. To do so, we first fit functions to the values of the coefficients at the maximum value for R_ρ that was considered ($R_\rho = 4$). It is helpful to anchor the functional dependence to the maximum value of R_ρ because of the asymmetry of the coefficients in figure 9. Specifically, we assign $f_1(R_d) = A_l(R_d, R_\rho = 4)$ and $f_2(R_d) = A_l(R_d, R_\rho = 4) + B_l(R_d, R_\rho = 4)$. As shown in figure 3.1(a), the best linear fit of f_1 to the data is

$$f_1 = 0.4R_d - 0.4474. \tag{3.1}$$

Figure 3.1(b) shows that f_2 is quadratic in R_d, which is fit by

$$f_2 = -0.1342R_d^2 + 0.3514R_d - 0.3646. \tag{3.2}$$

In addition, we find that $A_l - f_1$ for different R_d collapses reasonably well onto a master curve as shown in figure 3.2(a), which is expressed as

$$A_l - f_1 = 0.35e^{-2R_\rho}. \tag{3.3}$$

Similarly, $(A_l + B_l - f_2)/R_d$ data collapses onto a master curve as shown in figure 3.2(b), which takes the form

$$\frac{A_l + B_l - f_2}{R_d} = 0.43e^{-0.2R_\rho} - 0.2, \tag{3.4}$$

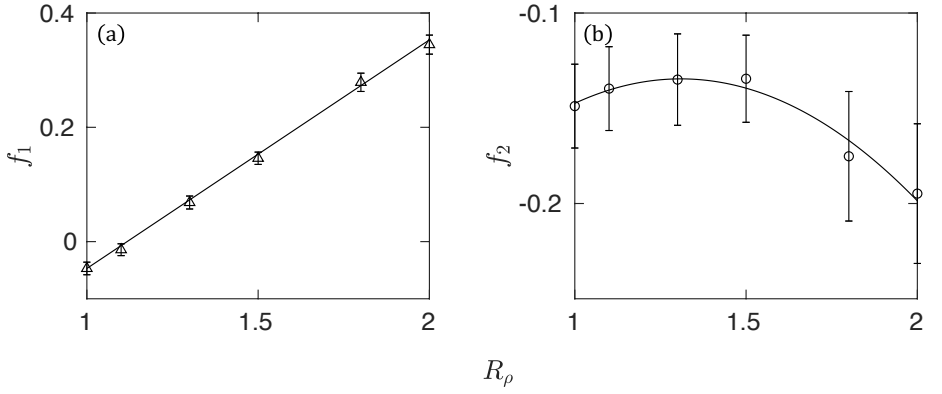

FIGURE 3.1. (a) $f_1 = A_l(R_d, R_\rho = 4)$ and (b) $f_2 = A_l(R_d, R_\rho = 4) + B_l(R_d, R_\rho = 4)$ vs. R_d. Data points correspond to those for $R_\rho = 4$ in figure 9. Line and curve are fits to the data as shown in equations (3.1) and (3.2), respectively.

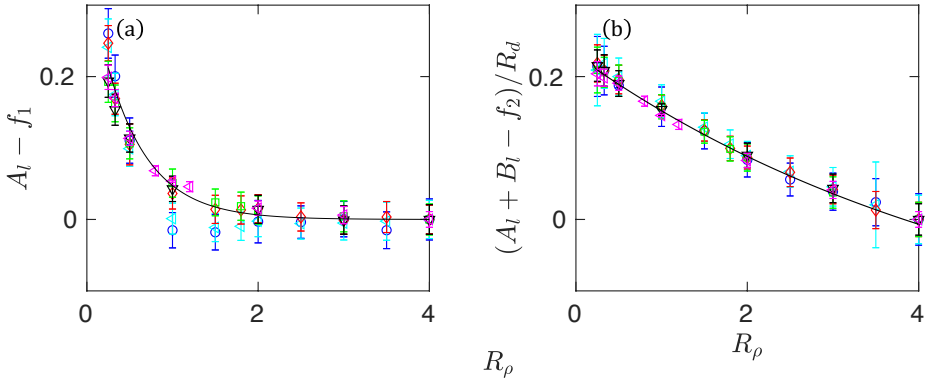

FIGURE 3.2. (a) $A_l - f_1$ and (b) $(A_l + B_l - f_2)/R_d$ vs. R_ρ. Different symbols correspond to those in figure 9. Curves are fits to the data as shown in equations (3.3) and (3.4).

Combining these results, the segregation model coefficients can be estimated as

$$A_l = 0.35e^{-2R_\rho} + f_1, \tag{3.5}$$

and

$$B_l = (0.43e^{-0.2R_\rho} - 0.2)R_d - A_l + f_2. \tag{3.6}$$

For the monodisperse condition $R_d = 1$ and $R_\rho = 1$, the empirical equations (3.1, 3.2, 3.5, 3.6) result in $A_l \approx 0$ and $B_l \approx 0$, as should be the case.

4. Mean velocity

Figure 4.1 shows that the streamwise velocity, u, predicted by the kinematic model [equation (4.2)] matches the DEM simulation results well at all five depths except near the feed-zone ($x/L < 0.1$), as expected. This is because in a rotated reference frame as shown in figure 1, upstream particles at deeper positions are directly beneath the feed-zone, such that the flow kinematics are affected by falling particles. The nearly linear decrease of u with x/L for $0.2 < x/L < 0.8$ indicates a uniform deposition of

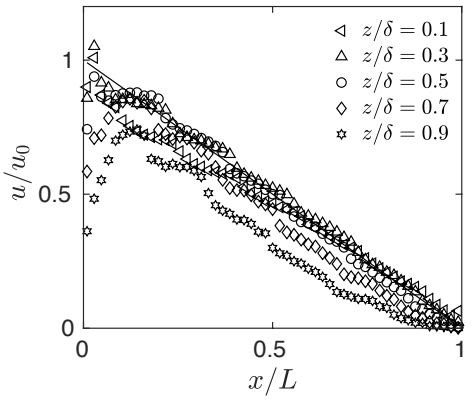

FIGURE 4.1. Streamwise velocity profiles at different depths. Symbols represent simulation data and line is prediction of equation (4.2). The streamwise velocity u is scaled by u_0, where $u_0 = u_{x=0,z}$ is calculated from equation (4.2). $R_d = 2$, $R_\rho = 4$, $\hat{c}_l = 0.5$, $q = 20\,\mathrm{cm}^2/\mathrm{s}$, $\delta = 1.5\,\mathrm{cm}$, and $L = 52\,\mathrm{cm}$.

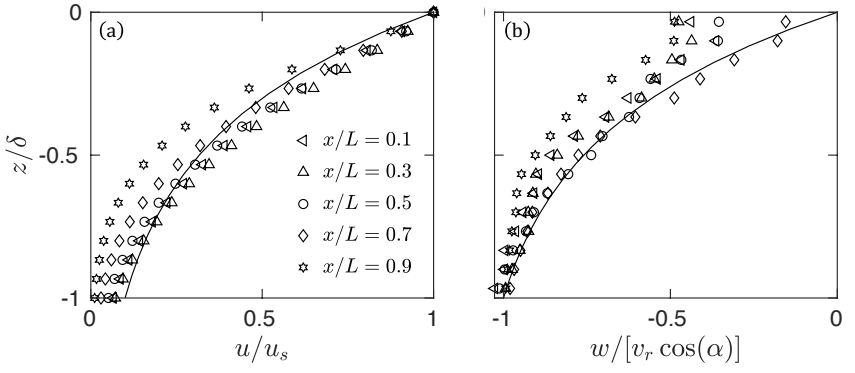

FIGURE 4.2. Streamwise and normal velocity profiles at different positions along the heap. Symbols represent simulation data and curves are predictions of equations (4.2) and (4.3). Velocities are scaled by u_s and $v_r\cos(\alpha)$ in the (a) streamwise and (b) normal directions, respectively, where u_s is the surface velocity measured from the simulation and $v_r\cos(\alpha)$ is the rise velocity of the heap surface.

particles on the heap, consistent with a nearly constant flowing layer thickness away from endwalls as shown in figure 3(a). Reasonably good agreement between the kinematic model prediction and simulation is also observed for u and normal velocity w as functions of z/δ at different streamwise positions in figure 4.2(a) and (b), respectively. For both cases, the discrepancies are slightly larger for $x/L = 0.9$ due to the decreasing flowing layer thickness near the downstream endwall.

5. Gravitational effect on free surface flow segregation

Segregation models by Marks *et al.* (2012), Tunuguntla *et al.* (2014), and Gray & Ancey (2015) indicate that the segregation flux is proportional to $g\cos\alpha$. Note that this is different from our model for free surface flows in which the segregation model coefficients A_i and B_i in equation (3.1) are not specified as functions of g or α. To characterize the

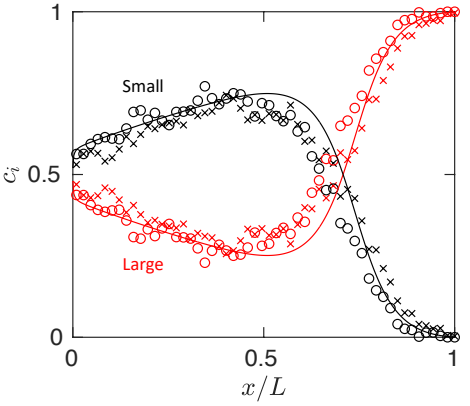

FIGURE 5.1. Streamwise particle concentration profiles from DEM simulations (symbols) and model (curves). The two sets of data correspond to $g = 9.81\,\mathrm{m/s^2}$ (○) and $4.91\,\mathrm{m/s^2}$ (×). $\hat{c}_l = 0.5$, $R_d = 1.5$, and $R_\rho = 1$.

influence of $g\cos\alpha$, figure 5.1 plots the streamwise particle concentration profiles from DEM simulations for an example case with two different values of g. These results show that reducing g by half has minimal influence on the segregation in the DEM simulations, consistent with our model prediction. This is also consistent with our previous size or density only segregation model's lack of dependence on g, which is robust in different flow geometries (rotating tumbler, 3D heap, hopper discharge) and with different particle properties, regardless of the repose angle α (Umbanhowar *et al.* 2019). The reasons behind this lack of dependence on $g\cos\alpha$ are beyond the scope of this study, but one possible explanation is that both the partial pressure and the inter-species drag are proportional to $g\cos\alpha$ through the lithostatic pressure, and thereby offset one another (Duan *et al.* 2020).

REFERENCES

Cai, R., Xiao, H., Zheng, J. & Zhao, Y. 2019 Diffusion of size bidisperse spheres in dense granular shear flow. *Phys. Rev. E* **99** (3), 032902.

Cundall, P. A. & Strack, O. D. L. 1979 A discrete numerical model for granular assemblies. *Géotechnique* **29** (1), 47–65.

Duan, Y., Umbanhowar, P. B., Ottino, J. M. & Lueptow, R. M. 2020 Segregation models for density-bidisperse granular flows. *Phys. Rev. Fluids* **5**, 044301.

Fan, Y., Umbanhowar, P. B., Ottino, J. M. & Lueptow, R. M. 2015 Shear-rate-independent diffusion in granular flows. *Phys. Rev. Lett.* **115** (8), 088001.

Gray, J. M. N. T. & Ancey, C. 2015 Particle-size and-density segregation in granular free-surface flows. *J. Fluid Mech.* **779**, 622–668.

Marks, B., Rognon, P. & Einav, I. 2012 Grainsize dynamics of polydisperse granular segregation down inclined planes. *J. Fluid Mech.* **690**, 499–511.

Shäfer, J., Dippel, S. & Wolf, D. E. 1996 Force schemes in simulations of granular materials. *J. Phys. I* **6** (1), 5–20.

Tunuguntla, D. R., Bokhove, O. & Thornton, A. R. 2014 A mixture theory for size and density segregation in shallow granular free-surface flows. *J. Fluid Mech.* **749**, 99–112.

Umbanhowar, P. B., Lueptow, R. M. & Ottino, J. M. 2019 Modeling segregation in granular flows. *Annu. Rev. Chem. Biomol. Eng.* **10**, 129–153.

Weinhart, T., Orefice, L., Post, M., van Schrojenstein Lantman, M. P., Denissen, I. F. C., Tunuguntla, D. R., Tsang, J. M. F., Cheng, H., Shaheen, M. Y., Shi, H., Rapino, P., Grannonio, E., Losacco, N., Barbosa, J., Jing, L., Alvarez Naranjo, J. E., Roy, S., den Otter, W. K. & Thornton, A. R. 2020 Fast, flexible particle simulations—an introduction to MercuryDPM. *Comput. Phys. Commun.* **249**, 107129.